All-Electric Spacecraft Precision Pointing using Model Predictive Control

Mirko Leomanni*, Andrea Garulli[†], Antonio Giannitrapani[‡] *Università di Siena, Siena, 53100, Italy*

Fabrizio Scortecci§

Aerospazio Tecnologie s.r.l., Rapolano Terme, Siena, 53040, Italy

Recent technological advances in the development of electric propulsion pave the way to the successful diffusion of all-electric spacecraft. Nevertheless, attitude control systems (ACS) accounting for the peculiarities of electric thrusters have still to be devised. This paper develops an ACS for spacecraft equipped with on/off xenon microthrusters. The number of thruster firings, which has a key impact on the thruster lifetime, is explicitly taken into account in the control design phase. By adopting a model predictive control (MPC) approach, a cost functional including both fuel consumption and number of firing cycles is minimized at each time step, within a receding horizon scheme. The effectiveness of the proposed ACS is validated on a sample geostationary mission and its performance is compared with different control laws involving on/off actuators.

I. Introduction

All-electric spacecraft, using EP systems for attitude control, have been studied since the early 1960's. The potential application of Teflon pulsed plasma thruster for attitude control has been

^{*}Ph.D, Dipartimento di Ingegneria dell'Informazione e Scienze matematiche, leomanni@dii.unisi.it

[†]Professor, Dipartimento di Ingegneria dell'Informazione e Scienze matematiche, garulli@dii.unisi.it

[‡]Assistant Professor, Dipartimento di Ingegneria dell'Informazione e Scienze matematiche, giannitrapani@dii.unisi.it

[§]Chairman, Aerospazio Tecnologie, fscortecci@aerospazio.com

investigated in [1], and later demonstrated in space by the NASA mission EO-1 [2]. An attitude control system based on high efficiency multistage plasma thrusters, exploiting a common xenon bus shared with the orbit maneuvering system, has been proposed in [3], for the specific requirements of the scientific mission GEO-Oculus. Another viable technology is represented by cold gas and resistojet thrusters which, besides using a single propellant bus for the whole control system, allow one to reduce complexity and cost of commercial platforms due to their inherent simplicity [4,5]. Cold gas and electrothermal microthrusters, with thrust levels scaled down to the millinewton range, are particularly well suited for precise attitude control, providing very small impulse bits and a minimal excitation of the spacecraft flexible modes. While the poor fuel efficiency of cold gas systems restricts their use to operational environment where the delta-v budget is considerably low, the foreseen availability of very high temperature resistojet and hollow cathode technologies, providing a substantial increase of the thruster specific impulse, raises the possibility of replacing existing momentum exchange devices with simple, reliable and relatively inexpensive xenon microtrusters [6]. These thrusters must be operated in on/off mode, and restrictions on the duration and number of thruster firings have to be accounted for in the design of the attitude control system. In particular, the number of firing cycles has an impact on both the lifetime of the thrusters, due to valve wear, and on the performance of the control system, which is affected by transient effects on the actuator dynamics. Such technological limitations typically result in oscillating behaviors of the closed-loop system [7]. Since the amplitude of these oscillations is inversely proportional to the number of thruster firings, achieving precise attitude control while retaining an acceptable number of switching cycles is a challenging task.

A wide variety of control techniques have been proposed in the literature for ACS design based on on/off actuators, including bang-bang control [8], linear quadratic regulators (LQR) with pulse-width pulse-frequency modulators (PWPF) [9,10], mixed-integer linear programming (MILP) control allocation [11], and model predictive control (MPC) [12,13]. While many of these techniques explicitly account for minimum firing duration constraints, they do not address the problem of minimizing the overall number of thruster firings, which has a key impact on the lifetime of the thrusters and hence of the mission itself.

In this paper, a new approach to ACS design is presented for three-axis precision pointing of all-electric spacecraft. An MPC law is proposed, whose objective is to keep the spacecraft attitude and angular velocity within given bounds. The main advantage of this approach compared to traditional techniques is that the number of thruster firings, as well the overall fuel consumption, are explicitly taken into account in the control design. Simulations are reported to demonstrate the feasibility of the proposed solution for a sample geostationary (GEO) mission, and to evaluate the performance of the control law in comparison to an LQR controller with a PWPF modulator.

The paper is organized as follows. Section II describes the main features of the attitude control problem and introduces the attitude dynamic model. In Section III, the MPC-based attitude control law is derived. Section IV presents an example GEO mission on which the ACS is tested. The performance of the proposed solution is evaluated through numerical simulations in Section V. In Section VI, some conclusions are drawn and future directions of research are outlined.

II. Problem setting

A. Reference frames and notation

Three reference frames are used in this work. The first one is an Earth centered inertial (ECI) frame. The other two coordinate systems are moving frames centered at the spacecraft center of mass. The so called local-vertical/local-horizontal (LVLH) frame is oriented so that its Z axis is aligned with the nadir vector, the Y axis is normal to the orbital plane and the X axis completes an orthogonal right handed frame. The body frame, whose axes are conventionally referred to as roll, pitch and yaw axes, is aligned with the principal axes of inertia of the spacecraft. The desired attitude during the spacecraft orbital motion is such that the body and the LVLH frame overlap.

Vector and matrices are denoted by boldface symbols. The symbol $\mathbf{0}$ denotes a vector whose components are all equal to 0. Similarly, $\mathbf{1}$ is a vector whose components are all equal to 1. The identity matrix of order n is denoted by \mathbf{I}_n . Diag and blockdiag denote the diagonal and blockdiagonal matrices, and the 1-norm and ∞ -norm of a vector $\mathbf{x} \in \mathbb{R}^n$ are defined as $\|\mathbf{x}\|_1 = \sum_{i=1}^n |x_i|$ and $\|\mathbf{x}\|_{\infty} = \max\{|x_i| \dots |x_n|\}$, respectively. The orientation of reference frame B with respect to reference frame A is expressed by the rotation matrix \mathbf{R}_{AB} or, equivalently, by the quaternion

 \mathbf{q}_{AB} . The scalar portion of the quaternion is the first element and the quaternion multiplication is defined such that $\mathbf{q}_{AC} = \mathbf{q}_{BC} \circ \mathbf{q}_{AB}$ corresponds to the sequence of rotations $\mathbf{R}_{AC} = \mathbf{R}_{BC} \mathbf{R}_{AB}$. The transformation from a quaternion to a rotation matrix is denoted by $\mathbf{R}(\mathbf{q})$. Small rotations are represented in quaternion form as $\delta \mathbf{q}(\gamma) = [1, \gamma^T/2]^T$, where γ is a three-dimensional rotation vector, and the skew-symmetric matrix constructed from a vector $\boldsymbol{\omega}$ is denoted by $\boldsymbol{\omega}^{\times}$.

B. Attitude control requirements

The objective of this work is to provide high accuracy attitude control of an all-electric platform, by means of an efficient rejection of the disturbance torques. Such torques arise from the interaction of environmental perturbations with the mass distribution and the geometric properties of the spacecraft, as well as from the uncertainty on the position of the center of mass and on the alignment of the orbit control thrusters used to perform station-keeping (SK) maneuvers.

The attitude control accuracy is typically dictated by the spacecraft payload. While a pointing accuracy below a prescribed value is the driving requirement for telecommunications, an additional constraint on the pointing rate accuracy is often enforced for Earth observation purposes. These requirements are expressed by the maximum allowed deviation of the spacecraft attitude and angular rate from the reference.

A number of technological limitations have to be accounted for in the design of a reaction control system based on on-off thrusters, the most significant ones being the propellant consumption necessary to generate control torques and the maximum number of cycles which can be delivered by the switching valves during thruster lifetime. An efficient attitude control scheme must then focus on simultaneously minimizing the fuel consumption and the number of thruster firings, while at the same time enforcing the attitude and angular rate accuracy requirements.

C. Attitude dynamics

Let \mathbf{q}_{IB} be the quaternion representing the orientation of the spacecraft body frame with respect to the ECI frame, and ω be the angular rate of the body frame with respect to ECI frame, expressed

in the body frame. The model describing the spacecraft attitude dynamics can be written as

$$\dot{\mathbf{q}}_{IB} = \frac{1}{2} \begin{bmatrix} 0 & \omega \end{bmatrix}^T \circ \mathbf{q}_{IB} \tag{1}$$

$$\dot{\omega} = \mathbf{I}_{\mathrm{M}}^{-1} \left(\tau_{d} + \tau_{u} - \omega \times \mathbf{I}_{\mathrm{M}} \, \omega - \dot{\mathbf{I}}_{\mathrm{M}} \, \omega \right), \tag{2}$$

where $\mathbf{I}_{\mathbf{M}}$ is the spacecraft inertia matrix, τ_d accounts for the disturbance torques and τ_u is the control torque (both expressed in the body frame). The mapping between the control torque τ_u and the thruster on/off activation command \mathbf{u} is given by a suitable matrix \mathbf{T} such that $\tau_u = \mathbf{T} \mathbf{u}$, where $\mathbf{u} = [u_1, ..., u_n]^T$ and $u_i \in \{0, 1\}$. The propellant mass rate, resulting from thruster operation, is

$$\dot{m} = -\frac{\bar{f} \parallel \mathbf{\Lambda} \mathbf{u} \parallel_1}{g I_{sp}}, \tag{3}$$

where g is the gravity acceleration, \bar{f} is the nominal thrust exerted by a single actuator, I_{sp} is the thruster specific impulse and Λ accounts for the specific thruster layout.

III. Attitude control

The purpose of the ACS is to track a reference attitude trajectory consisting of: (i) the quaternion $\bar{\mathbf{q}}_{IL}$, which is periodically uploaded from ground stations and defines the orientation of the LVLH frame with respect to the ECI frame; (ii) the LVLH frame rotation rate, given by $\bar{\omega}_L = [0, -\omega_L, 0]^T$, where ω_L is the angular rate about the pitch axis.

A. Error dynamics

A discrete-time linear approximation of the attitude error dynamics is derived for control purposes. Assuming that the attitude error with respect to the reference LVLH frame is small, it can be approximated by the three-dimensional rotation vector $\delta\theta$, which is obtained from the vector part of the attitude error quaternion as

$$\begin{bmatrix} 1 & \delta \boldsymbol{\theta}/2 \end{bmatrix}^T = \delta \mathbf{q}(\delta \boldsymbol{\theta}) \approx \mathbf{q}_{IB} \circ \bar{\mathbf{q}}_{LI}, \qquad (4)$$

where the right hand side represents the rotation from the LVLH frame to the body frame. The angular rate error is given by the difference between the body frame and the LVLH frame rotation rates,

$$\delta\omega = \omega - \bar{\omega}_L. \tag{5}$$

Assuming small angles and small angular rates, one has $\delta \dot{\theta} = \delta \omega - \bar{\omega}_L^{\times} \delta \theta$. Hence, the linearized model can be cast in state space form as

$$\dot{\mathbf{x}} = \mathbf{A}\,\mathbf{x} + \mathbf{B}\,\mathbf{u} + \mathbf{B}_d\,\boldsymbol{\tau}_d,\tag{6}$$

where $\mathbf{x} = [\delta \theta^T \delta \omega^T]^T$. The state matrix is given by

$$\mathbf{A} = \begin{bmatrix} -\bar{\omega}_L^{\times} & \mathbf{I}_3 \\ \mathbf{0}_3 & \mathbf{A}' \end{bmatrix},\tag{7}$$

where $\bar{\omega}_L^{\times}$ and \mathbf{A}' represent the cross-coupling contribution due to the rotation of the LVLH frame. By using a constant approximation of the inertia matrix

$$\bar{\mathbf{I}}_{\mathbf{M}} = \operatorname{diag}(I_{x}, I_{y}, I_{z}), \tag{8}$$

through long but standard manipulations of (1),(2) and (5) (see, e.g., [14]), one obtains

$$\mathbf{A}' = \begin{bmatrix} 0 & 0 & \frac{I_z - I_y}{I_x} \, \omega_L \\ 0 & 0 & 0 \\ \frac{I_y - I_x}{I_z} \, \omega_L & 0 & 0 \end{bmatrix}. \tag{9}$$

The input matrices can be expressed as

$$\mathbf{B} = \begin{bmatrix} \mathbf{0}_{n \times 3} & \overline{\mathbf{I}}_{\mathbf{M}}^{-1} \mathbf{T} \end{bmatrix}^{T}, \qquad \mathbf{B}_{d} = \begin{bmatrix} \mathbf{0}_{3} & \overline{\mathbf{I}}_{\mathbf{M}}^{-1} \end{bmatrix}^{T}. \tag{10}$$

The continuous time model is discretized with a sampling time Δt_s , thus obtaining

$$\mathbf{x}(t+1) = \mathbf{F}\,\mathbf{x}(t) + \mathbf{G}\,\mathbf{u}(t) + \mathbf{G}_d\,\boldsymbol{\tau}_d(t),\tag{11}$$

with
$$\mathbf{F} = e^{\mathbf{A}\Delta t_s}$$
, $\mathbf{G} = \left(\int_0^{\Delta t_s} e^{\mathbf{A}\rho} d\rho\right) \mathbf{B}$ and $\mathbf{G}_d = \left(\int_0^{\Delta t_s} e^{\mathbf{A}\rho} d\rho\right) \mathbf{B}_d$.

B. Control design

The proposed ACS is based on an MPC approach, which explicitly incorporates the limitations on pointing and pointing rate accuracy. A suitable trade-off between fuel consumption and number of thruster firings is introduced in the cost function. Due to the presence of linear performance indexes and on/off actuators, the problem requires the solution of a mixed-integer linear program within a receding horizon control scheme. The control accuracy requirements can be formulated using the following constraints:

$$\|\mathbf{K}_{\theta} \delta \boldsymbol{\theta}\|_{\infty} \leq 1$$

$$\|\mathbf{K}_{\omega} \delta \boldsymbol{\omega}\|_{\infty} \leq 1,$$
(12)

where the diagonal weighting matrices \mathbf{K}_{θ} and \mathbf{K}_{ω} account for proper scaling of the attitude and angular rate errors. According to (3), a cost function proportional to the amount of expended fuel from time t to time $t + N_u$ is given by:

$$J_1(\mathbf{U}) = \sum_{k=0}^{N_u} \| \mathbf{\Lambda} \mathbf{u}(t+k) \|_1,$$
 (13)

where $\mathbf{U} = \{\mathbf{u}(t), \dots, \mathbf{u}(t + N_u)\}$ is the input sequence on the considered control horizon. Moreover, being $u_i \in \{0, 1\}$, the number of thruster switchings, which accounts for thruster valve wear, can be expressed as:

$$J_2(\mathbf{U}) = \sum_{k=0}^{N_u} \| \mathbf{\Lambda} [\mathbf{u}(t+k) - \mathbf{u}(t+k-1)] \|_1.$$
 (14)

Given a state vector $\mathbf{x}(t)$, the computation of the control input sequence \mathbf{U} at time t can be formulated as an optimization problem of the form:

$$\min_{\mathbf{U}} \quad (1-\alpha) J_1(\mathbf{U}) + \alpha J_2(\mathbf{U})$$
s.t.
$$\mathbf{x}(t+k+1) = \mathbf{F} \mathbf{x}(t+k) + \mathbf{G} \mathbf{u}(t+k) + \mathbf{G}_d \boldsymbol{\tau}_d(t+k)$$

$$\|\mathbf{D} \mathbf{x}(t+k)\|_{\infty} \le 1$$

$$\mathbf{M} \mathbf{u}(t+k) \le \mathbf{1}$$

$$u_i(t+k) \in \{0, 1\} \quad \forall i, \forall k = 0, \dots, N_u,$$
(15)

where $\alpha \in [0, 1]$ is a relative weight of the terms J_1 and J_2 , $\mathbf{D} = \text{blockdiag}(\mathbf{K}_{\theta}, \mathbf{K}_{\omega})$ accounts for control accuracy requirements, and the matrix \mathbf{M} is included to account for control allocation constraints.

In a receding horizon control strategy (see, e.g., [15]), one has to solve problem (15) at each time t and then apply the first element of the computed input sequence, which hereafter will be denoted by $\mathbf{U}_{t+N_u|t} = \{\mathbf{u}(t|t), \dots, \mathbf{u}(t+N_u|t)\}$. Hence, the instantaneous thruster activation command is given by $\mathbf{u}(t) = \mathbf{u}(t|t)$. In order to solve problem (15), the initial state $\mathbf{x}(t)$ and of the disturbance term $\tau_d(t+k)$, $k=0,\dots,N_u-1$ should be available. Since these quantities are not known, one has to resort to a navigation algorithm to estimate them. To this aim, a suitable extended Kalman filter (EKF) filtering algorithm is adopted (see Section III.C). In order to ensure feasibility in the presence of estimation errors and model uncertainties, the state constraints in problem (15) are relaxed by introducing slack variables and penalizing them in the cost function. Such relaxation is motivated by the fact that small violations of the error constraints can be tolerated for short time periods, provided that slightly conservative bounds on the pointing and pointing rate accuracy are

used. Hence, problem (15) can be reformulated as

$$\min_{\mathbf{U}_{t}, \mathbf{S}} (1 - \alpha) J_{1}(\mathbf{U}_{t+N_{u}|t}) + \alpha J_{2}(\mathbf{U}_{t+N_{u}|t})
+ \sum_{k=1}^{N-1} || \mathbf{K}_{s} \mathbf{s}(t+k) ||_{1} + || \mathbf{K}_{x} \mathbf{x}(t+N|t) ||_{1}
s.t. $\mathbf{x}(t|t) = \hat{\mathbf{x}}(t)$

$$\mathbf{x}(t+k+1|t) = \mathbf{F} \mathbf{x}(t+k|t) + \mathbf{G} \mathbf{u}(t+k|t) + \mathbf{G}_{d} \hat{\boldsymbol{\tau}}_{d}(t+k)
- \mathbf{1} - \mathbf{D} \mathbf{s}(t+k) \leq \mathbf{D} \mathbf{x}(t+k|t) \leq \mathbf{1} + \mathbf{D} \mathbf{s}(t+k)$$

$$\mathbf{s}(t+k) \geq \mathbf{0}$$

$$\mathbf{M} \mathbf{u}(t+k|t) \leq \mathbf{1}$$

$$u_{i}(t+k|t) \in \{0, 1\} \qquad \forall i, \forall k = 0, ..., N-1$$

$$\mathbf{u}(t+N_{u}+1|t) = ... = \mathbf{u}(t+N-1|t) = \mathbf{0},$$$$

where $\hat{\mathbf{x}}(t)$ is the estimate of the error state vector $\mathbf{x}(t)$ returned by the EKF. The weight on the terminal state \mathbf{K}_x is a standard tool in MPC, which favours stability of the receding horizon control strategy [16], while matrix \mathbf{K}_s is introduced to penalize the weighted ℓ_1 -norm of the the slack variables $\mathbf{S} = \{\mathbf{s}(t+1), \dots, \mathbf{s}(t+N-1)\}$. It is worth noticing that in problem (16), the control horizon N_u is different from the prediction horizon N_s , with $N_u \leq N-1$, on which the state constraints are enforced. After the first N_u samples, the control variables are set to zero while the state constraints must be satisfied also in the subsequent $N-N_u-1$ samples. This allows one to suitably trade-off the number of optimization variables and the performance of the ACS. In fact, problem (16) is a MILP problem which is known to be computationally intractable in the general case. Nevertheless, if the control horizon is kept short enough, state-of-the-art MILP algorithms can provide an approximate solution in a reasonable amount of time.

C. Navigation

A continuous/discrete multiplicative extended Kalman filter is adopted for autonomous navigation (see e.g. [17]). The filter processes data from a star tracker and a set of three orthogonal gyros

to estimate the attitude of the spacecraft and the resultant of the disturbance torques. The output of the star-tracker is a quaternion of the form $\check{\mathbf{q}}_{IB} = \delta \mathbf{q}(\mathbf{w}_q) \circ \mathbf{q}_{IB}$, where \mathbf{w}_q is the measurement noise. Gyro measurements are modeled as $\check{\boldsymbol{\omega}} = \boldsymbol{\omega} + \mathbf{b}_{\omega} + \mathbf{w}_{\omega}$, where $\boldsymbol{\omega}$ is the true angular rate, \mathbf{w}_{ω} is the measurement noise and \mathbf{b}_{ω} is the gyro bias. The gyro bias can be modeled as a random walk process, as

$$\dot{\mathbf{b}}_{\omega} = \mathbf{w}_{b},\tag{17}$$

where \mathbf{w}_b is the rate random walk noise. The state of the filter includes the angular rate dynamics, in order to provide an estimate $\hat{\tau}_d$ of the disturbance torques. Since the most significant torques depend on thruster misalignment during SK, they can be assumed to be constant over the control horizon of problem (16). Hence, τ_d is treated as an unknown parameter to be estimated by the EKF.

Using a constant approximation of the inertia matrix of the form (8), the filter state propagation model is obtained from eqs. (1), (2) and (17) as

$$\dot{\hat{\mathbf{q}}}_{IB} = \frac{1}{2} \begin{bmatrix} 0 & \hat{\boldsymbol{\omega}} \end{bmatrix}^T \circ \hat{\mathbf{q}}_{IB}
\dot{\hat{\boldsymbol{\omega}}} = \bar{\mathbf{I}}_{M}^{-1} \left(\hat{\boldsymbol{\tau}}_d + \bar{\boldsymbol{\tau}}_u - \hat{\boldsymbol{\omega}} \times \bar{\mathbf{I}}_{M} \hat{\boldsymbol{\omega}} \right)
\dot{\hat{\mathbf{b}}}_{\omega} = \mathbf{0}_{3\times 1}, \quad \dot{\hat{\boldsymbol{\tau}}}_d = \mathbf{0}_{3\times 1},$$
(18)

where τ_u is the commanded control torque. To avoid covariance singularities due to the quaternion unit-norm constraint, the attitude estimation error is parameterized using a three-dimensional rotation vector [18]. The covariance matrix of the filter is propagated according to $\dot{\mathbf{P}} = \mathbf{JP} + \mathbf{PJ}^T + \mathbf{Q}$. Linearizing the state dynamics around the current estimate, the Jacobian matrix can be expressed as

$$\mathbf{J} = \begin{bmatrix} -\hat{\boldsymbol{\omega}}^{\times} & \mathbf{I}_{3} & \mathbf{0}_{3} & \mathbf{0}_{3} \\ \mathbf{0}_{3} & \mathbf{J}' & \mathbf{0}_{3} & \mathbf{I}_{M}^{-1} \\ \hline & \mathbf{0}_{6\times12} \end{bmatrix}, \tag{19}$$

where $\hat{\boldsymbol{\omega}} = [\hat{\omega}_x, \ \hat{\omega}_y, \ \hat{\omega}_z]^T$, and

$$\mathbf{J'} = \begin{bmatrix} 0 & \frac{I_y - I_z}{I_x} \, \hat{\omega}_z & \frac{I_y - I_z}{I_x} \, \hat{\omega}_y \\ \frac{I_z - I_x}{I_y} \, \hat{\omega}_z & 0 & \frac{I_z - I_x}{I_y} \, \hat{\omega}_x \\ \frac{I_x - I_y}{I_z} \, \hat{\omega}_y & \frac{I_x - Iy}{I_z} \, \hat{\omega}_x & 0 \end{bmatrix}. \tag{20}$$

The process noise covariance is given by the block diagonal matrix $\mathbf{Q} = \text{blockdiag } (\mathbf{0}_3, \mathbf{Q}_\omega, \mathbf{Q}_b, \mathbf{Q}_\tau)$, where \mathbf{Q}_ω accounts for inertia, thruster noise and alignment uncertainties, $\mathbf{Q}_b = E\left[\mathbf{w}_b(t) \ \mathbf{w}_b(t')^T\right]$ and \mathbf{Q}_τ is set to different values for station-keeping and free orbit drift to model the expected level of uncertainty arising in each operational mode. When measurements are available, the attitude estimate is updated by using a multiplicative approach, while the classical update equations are adopted for the other states.

IV. Reference mission

In order to demonstrate the feasibility of the proposed solution, the ACS is applied to a sample GEO mission with the following orbit parameters: semi-major axis 42165 km, inclination \in [0, 0.05] deg, longitude \in [75.05, 75.15] deg, eccentricity \simeq 0. The spacecraft has the typical layout of a small two tons GEO platform, see e.g. [19]. The size of the main body is $2 \text{ m} \times 2 \text{ m} \times 2.5 \text{ m}$ and two solar panels of dimensions $5 \text{ m} \times 2 \text{ m}$ are attached to the north and south faces of the bus, providing 4.5 kW of average power.

The considered propulsion system is illustrated in Fig. 1. Four SPT-100 Hall effect thruster (HET) modules (EP1, EP2, EP3, EP4) symmetrically oriented around the nadir vector, with an angle of 45° between the North/South axis and the thrust direction, are used for SK maneuvers. Nominally, the EP thrust vectors are aligned with the center of mass of the spacecraft. Eight on/off xenon microthruster modules that can be operated either as cold gas thrusters (CGT) or high temperature electrothermal thrusters (HTET) are used for real-time attitude control. Operation in HTET mode provides an increased specific impulse, which is expected in the 100 s region for both high temperature resistojets and up to 200 s for hollow cathode thrusters using xenon [20]. Four thrusters (AT1, AT2, AT3, AT4) are mounted on the anti-nadir face, with an angle of 48.5°

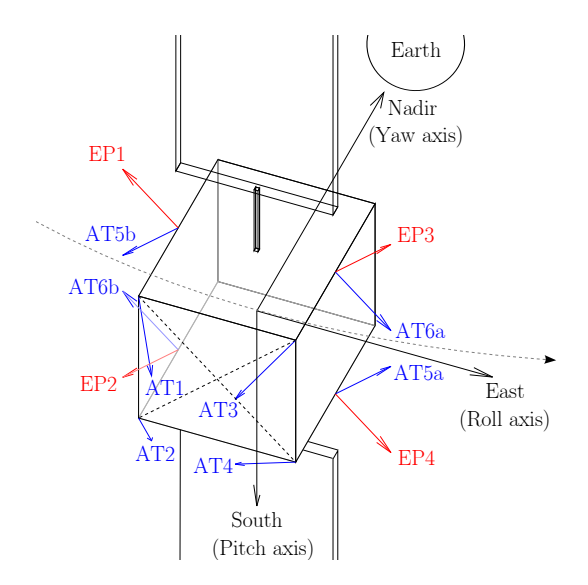


Figure 1. Thrusters layout

between the diagonal of the face and the thrust direction, to maximize the lever arm and hence the torque about both the roll and pitch axes. The remaining four thruster (AT5a, AT5b, AT6a, AT6b) are symmetrically oriented around the nadir vector, with an angle of 135° between the North/South axis and the thrust direction, and fired in pairs to provide pure torques around the yaw axis. Such configuration is fully compatible with thruster plume direction, torque level and power requirements of the considered mission. The basic specifications of the propulsion system are summarized in Table 1.

Table 1. Propulsion system specifications

Type	Thrust	I_{sp}	Power	Mass
HET	75 mN	1500 s	1350 W	3.5 kg
CGT/HTET	0.5/1.5 mN	30/90 s	< 60 W	< 0.3 kg

By simulating a weekly NSSK cycle, with one day devoted to orbit determination followed by six days of pre-planned maneuvers (see e.g. [21]), it turns out that the maximum magnitude of the SK disturbance torques is much greater than that of the environmental torques. For any possible combination of the actual center of mass position and EP thrust directions, the pitch and roll components of the SK disturbance torque are coupled and have approximately the same magnitude, while the yaw component, with a larger worst-case magnitude, is almost decoupled. Therefore, in order to efficiently reject such a disturbance, the thruster layout has been designed so that cou-

pled control torques of equal magnitude are produced around the roll and pitch axes, while the control torque around the yaw axis may be decoupled. The force generated by the attitude control thrusters mounted on the anti-nadir face of the bus represents a minor orbit perturbation, so that an eventual long-term contribution is easily compensated by sporadic EP maneuvers. Thrusters AT5a and AT5b, as well as thrusters AT6a and AT6b (see Fig. 1), are fired simultaneously. Hence, the thruster activation command can be denoted by $\mathbf{u} = [u_1, \dots, u_6]^T$, where u_1, \dots, u_4 are the command variables of thrusters AT1-AT4, while u_5 and u_6 control the AT5 and AT6 pairs of thrusters, and in (3) one has $\mathbf{\Lambda} = \text{diag}([1, 1, 1, 1, 2, 2])$. To avoid control torques summing up to zero, the simultaneous use of thrusters AT1-AT4, AT2-AT3 and AT5-AT6 is prevented by setting the constraint matrix \mathbf{M} in (15) to

$$\mathbf{M} = \begin{bmatrix} 1 & 0 & 0 & 1 & 0 & 0 \\ 0 & 1 & 1 & 0 & 0 & 0 \\ 0 & 0 & 0 & 0 & 1 & 1 \end{bmatrix}. \tag{21}$$

Thrusters are designed to be possibly operated in electrothermal mode, by ohmic heating of a resistance element. To retain an acceptable number of thermal cycles, the following operation regime is considered: (i) CGT mode operation of AT thrusters for attitude control during free orbit drift, when a low delta-v is required to counteract the environmental torques, (ii) HTET mode operation of AT thrusters for attitude control during SK maneuvers, providing increased thrust and I_{sp} for efficient compensation of additional EP-induced torques. A unique thermal cycle is performed for each SK maneuver.

The attitude control accuracy specifications (12) are summarized in Table 2, according to the typical requirements of a multi-mission platform, which includes Ka/Ku-band communication and Earth imaging payloads (see, e.g., [22]). Therein, the time interval in which SK maneuvers are not performed is referred as free orbit drift. Note that pointing rate accuracy requirements are relaxed for SK maneuvers, since Earth imaging is not performed during such operations. Also, note that control accuracy requirements for the yaw axis are less stringent than those for the roll and pitch axes, because the yaw pointing error does not directly affect the quality of communications and observations.

Table 2. Attitude control requirements

ACS requirements	Free orbit drift		Station-Keeping		
ACS requirements	Roll, Pitch	Yaw	Roll, Pitch	Yaw	
Pointing accuracy	0.5 mrad	1 mrad	0.5 mrad	1 mrad	
Rate accuracy	$1.5 \mu \text{rad/s}$	$3 \mu rad/s$	$10 \mu \text{rad/s}$	$20 \mu \text{rad/s}$	

V. Simulation results

A high-fidelity simulator has been developed, combining a realistic model of the spacecraft dynamics with a navigation system relying upon an EKF for state estimation, to evaluate the performance of the ACS. Table 3 summarizes the main simulation parameters. The deadband sizes

Table 3. Simulation parameters

Parameter	Value		
Center of mass offset	1.5 cm per axis		
Center of solar pressure offset	5 cm along the pitch axis		
EP thrust vector misalignment	0.6 deg half-cone		
AT thrust vector misalignment	0.1 deg half-cone		
EP and AT thrust noise	1 % of the nominal thrust		
Gyro measurement noise	$1 \mu \text{rad}/\sqrt{\text{s}} (3\sigma)$		
Star-tracker measurement noise	$0.1 \operatorname{mrad} (3\sigma)$		

 \mathbf{K}_{θ} and \mathbf{K}_{ω} in (12) are set according to the bounds reported in Table 2. The tuning parameters of the controller are $\Delta t_s N_u$, N_x , \mathbf{K}_x , and α in (16). A sampling time $\Delta t_s = 0.5 s$ has been chosen. Such a value is adequate for discretizing the spacecraft dynamic model and is well within the constraints on the minimum firing time imposed by the thruster technology. The control horizon N_u , which is proportional to the number of binary variables in the optimization problem, has the major impact on the real-time computational burden of the control system. Since the amount of computational resources available on-board a spacecraft is typically limited, $N_u = 3$ has been chosen. A prediction horizon three times longer than the control horizon has been selected, by setting $N_x = 9$. The penalty term \mathbf{K}_s , which affects the constraint violations, has been chosen as a block diagonal matrix $\mathbf{K}_s = \text{blockdiag}(5 \cdot 10^5 \, \mathbf{I}_3)$, $7 \cdot 10^5 \, \mathbf{I}_3$), while the terminal weight has been set to $\mathbf{K}_x = \text{blockdiag}(4 \cdot 10^3 \, \mathbf{I}_3, 1 \cdot 10^4 \, \mathbf{I}_3)$. Finally, the parameter α determines the relative

weight of the fuel consumption and the number of thruster firings in the cost function of the optimization problem. In order to find a suitable value of α , the ACS has been simulated with values of α ranging from zero to one. Since different control modes are defined according to mission requirements, free orbit periods lasting one day and NSSK maneuvers of 55 minutes duration have been simulated separately. A worst-case scenario has been considered, by assuming the maximum disturbance torque compatible with the uncertainty on the center of mass, center of solar pressure and thruster misalignment. The results are depicted in Fig. 2, where the fuel consumption and the number of thruster firings are reported for SK and free orbit drift periods. As expected, the parameter α allows one to trade-off between two objectives. It can be noticed that for both SK and free orbit drift the fuel consumption is approximately constant as long as α is smaller than 0.8, while it rapidly grows as α approaches 1. Conversely, an acceptable number of firings is achieved only if α is larger than 0.7. From these observations, $\alpha = 0.75$ has been selected. Fig. 2 also confirms that the major contribution to the attitude control delta-v budget is due to SK operations. Even if the microthrusters efficiency is increased by HTET mode operation, the fuel required for EP disturbance rejection of a single NSSK maneuver is still considerably higher than the fuel needed to compensate for one day of environmental torques using thrusters in CGT mode. The proposed combination of tuning parameters provides an average computational time of the control law in the millisecond range on a 2 GHz single-core CPU, by using the IBM ILOG CPLEX mixed-integer programming solver [23], based on a branch and bound algorithm.

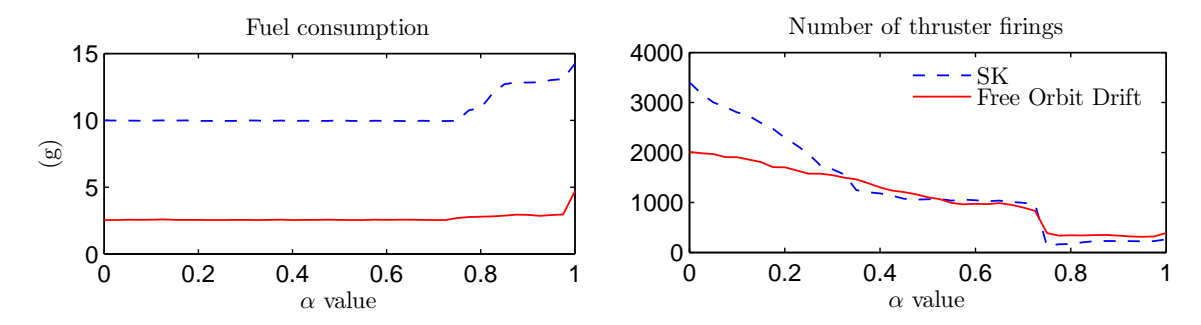


Figure 2. Tuning of parameter α

The steady state behaviour of the ACS is reported in Fig. 3, for a time interval of one week. The attitude tracking error remains always well enclosed within the bounds (dash-dotted lines) specified by the pointing accuracy requirements, and shows an oscillating trend that corresponds

to the disturbance torque profile, except from periodic spikes due to SK maneuvers or thruster operation within solar eclipses, when the environmental torques vanish resulting in closed-loop oscillations with the same amplitude of the deadband (due to the minimum impulse bit of the thrusters). Such kind of behaviour is typical for pulse-modulated thruster control systems with deadband. Similarly to what observed for the attitude error, the angular rate tracking error does not exceed the pointing rate accuracy bounds. The performance of the microthruster reaction system, in terms of fuel consumption (left) and number of firings cyles per thruster (right, where each line represents a single thruster), is reported in Fig. 4. The microthrusters are operated in CGT mode during free orbit drift and in HTET mode during SK maneuvers. The stair-step profile of the

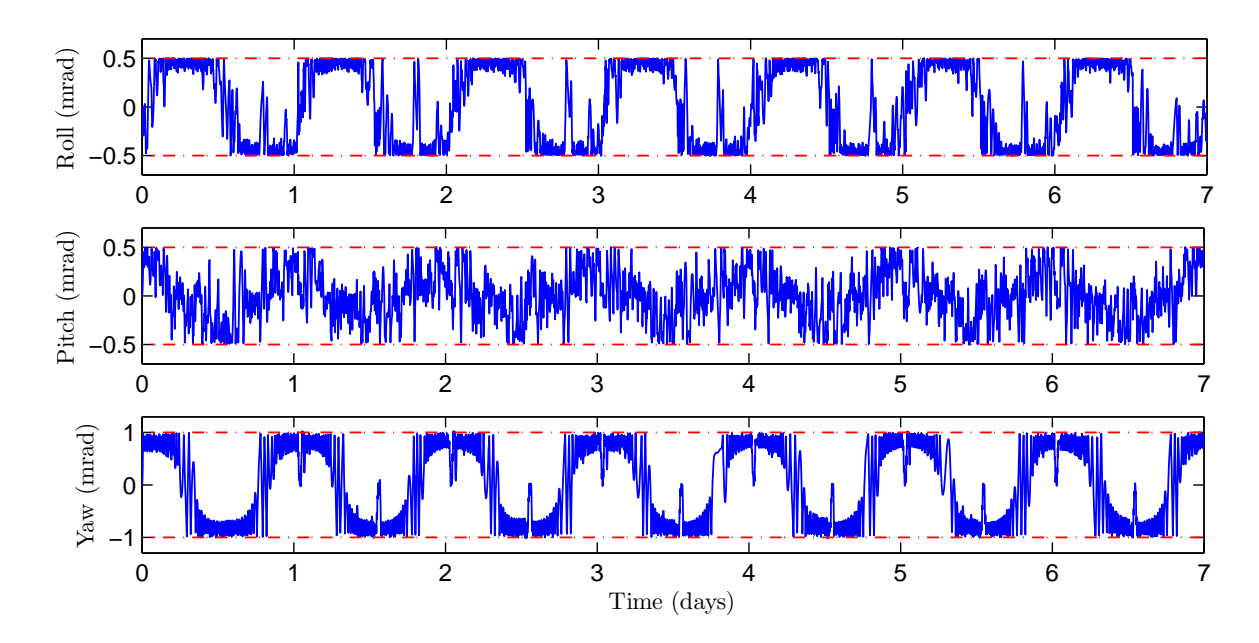


Figure 3. Pointing error

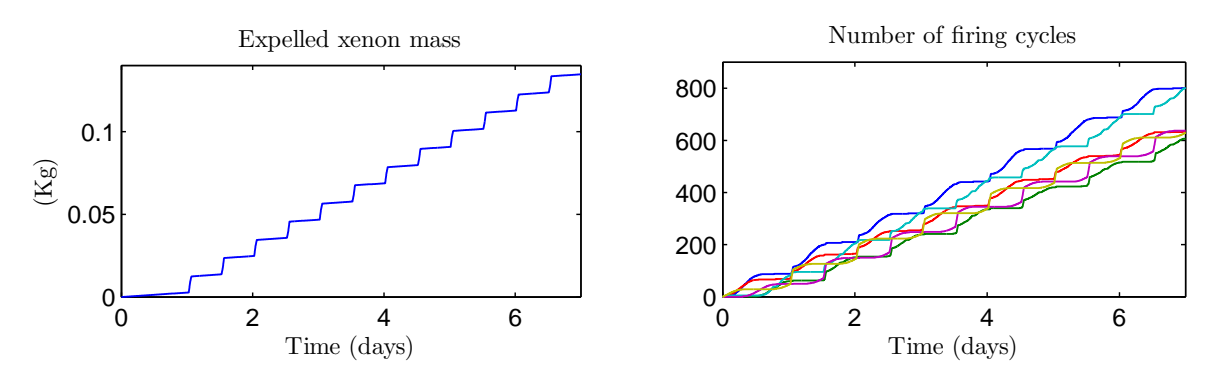


Figure 4. Microthruster reaction system performance

expelled fuel clearly indicates that the major contribution to the propellant budget is due to SK

disturbance rejection, as expected. The overall xenon mass required for precise attitude control is approximately 0.135 kg: 0.019 kg to counteract environmental disturbances and 0.116 kg to compensate for SK disturbance torques. The amount of firing cycles is fairly distributed among free orbit drift and SK periods, and grows regularly for each thruster. At the end of the simulation, about 800 on/off cycles are accumulated by thrusters AT1 and AT4, while a number of cycles between 600 and 650 is observed for the remaining thrusters. The overall firing time per thruster varies between 2.5 hr and 2.9 hr, about 85% of which being spent for SK disturbance rejection. Based on these results, Table 4 summarizes the performance of the reaction control system for a mission duration of 15 years. The total amount of xenon needed for microthruster operation represents a significant addition to the fuel budged of the mission, being the propellant mass required for 15 years of NSSK in the order of 150 kg for the HET thrusters considered in Table 1. However, considering that the typical mass of momentum-exchange devices, such as reaction wheels or control moment gyros, together with the xenon mass required for wheel desaturation, can easily exceed 50 kg, and that such systems are replaced by light-weight microthrusters, the overall penalty on the spacecraft mass is predicted in the 60 kg range. It is believed that this is a reasonable tradeoff as it allows one to remove moving and vibrating parts from the attitude control system, as well as to reduce its complexity and cost. Moreover, the results presented so far are obtained by using conservative propulsion system specifications, which ensure compatibility with different models of EP and HTET thrusters. In specific cases, where a better alignment of the EP thrust vector and/or an increased I_{sp} of the reaction thrusters can be guaranteed, a significant reduction of the propellant consumption is expected, since the amount of xenon required for EP torques compensation scales approximately linearly with these quantities. For instance, the performance reported in Table 5 is obtained for an EP thrust vector misalignment of 0.1 deg, as in [1,21], and an I_{sp} of 200 s, which is the target value for the development of the hollow cathode technology. Such a performance makes the proposed ACS a competitive alternative to systems based on momentum exchange devices. Finally, it must be observed that the firing time and the number of on/off and thermal cycles per thruster, given in Tables 4 and 5, are compatible with the considered CGT/HTET technology. In particular, the difference between the number of on/off and thermal cycles for HTET is due to the

Table 4. Propulsion system performance: EP thruster misalignment 0.6° , HTET $I_{sp}=90$

Type	Xenon mass	On/off cycles	Firing time	Thermal cycles
CGT	15 kg	350000	300 hr	-
HTET	91 kg	300000	2000 hr	10000
Total	106 kg	650000	2300 hr	10000

Table 5. Propulsion system performance: EP thruster misalignment 0.1° , HTET $I_{sp}=200$

Type	Xenon mass	On/off cycles	Firing time	Thermal cycles
CGT	15 kg	350000	300 hr	-
HTET	22.5 kg	380000	1100 hr	10000
Total	37.5 kg	730000	1400 hr	10000

fact that for each SK maneuver a single thermal cycle is performed, while several valve switchings are required to meet the desired control accuracy.

The proposed ACS has been compared to a LQR+PWPF scheme, consisting of the cascade of a LQR controller and a PWPF modulator, for SK disturbance rejection. The SK maneuver consists of firing a pair of thrusters in sequence around an orbit node. Therefore, the resulting disturbance torque, depending on the displacement of the thrust vectors with respect to the spacecraft center of mass, is piecewise constant: $\tau_{sk} = [1.6, 1.7, 2.7]^T$ mN·m during the first half of the maneuver, and $\tau_{sk} = [1.7, -1.6, 1.1]^T$ mN·m during the second half. In Fig. 5, it can be observed that both controllers succeed in keeping the errors within the maximum allowed deviation, for all axes (although the LQR law fails to keep the pitch and yaw rate transient within the bounds due to an impulsive variation of the disturbance torque at time t=1683 s). Clearly, an advantage of the MPC approach is that the error bounds are enforced directly as constraints in the optimization problem (16), while a trial-and-error procedure is necessary to suitably tune the parameters of the LQR+PWPF controller.

The performance of the two ACSs in terms of fuel consumption and number of thruster firings is reported in Fig. 6. The MPC scheme requires about 5% less fuel and 25% less thruster firings with respect to the LQR+PWPF one, mainly due to a more efficient management of the firing cycles for the cross-coupled axes (roll and pitch).

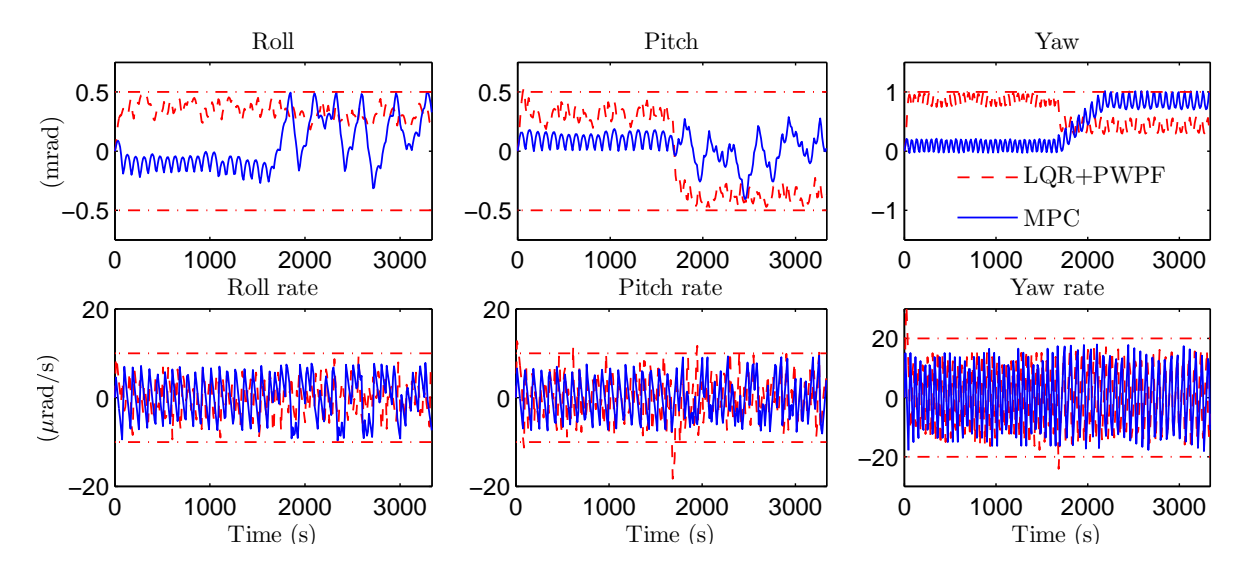


Figure 5. Tracking errors for a sample SK maneuver

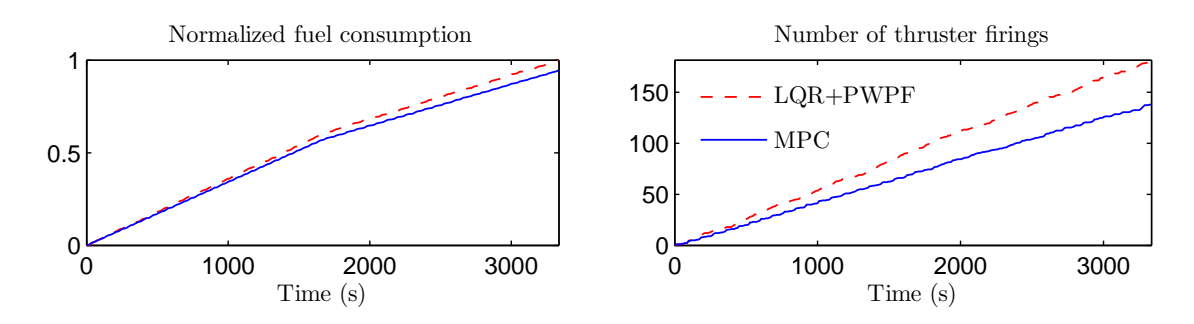


Figure 6. Fuel consumption and number of firings in comparison

VI. Conclusions

In this paper, an attitude control system for all-electric platforms equipped with xenon microthrusters has been presented. An MPC-based approach has been adopted, able to confine the pointing
and pointing rate tracking errors within prescribed bounds, while at the same time satisfying the
constraints imposed by the technological limitations of the actuators. The proposed methodology allows the designer to explicitly take into account both the fuel consumption and the number
of firings of the thrusters, providing a suitable way to trade-off these objectives by means of a
scalar parameter. The approach is general enough to be applied to the three-axis attitude control
problem, even in the presence of coupled dynamics. This is the case, for example, whenever nonorthogonal thruster configurations are adopted for maximizing the generated torque or satisfying
constraints coming from the spacecraft layout. Simulation results show that the achievable accuracy is suitable for both communication and Earth observation GEO missions. Moreover, the fuel

consumption and number of firing cycles makes the proposed ACS a viable alternative to systems based on momentum wheels.

From the computational viewpoint, it is worth remarking that the optimization problem involved in the computation of the control law is quite challenging. The computational burden is heavily affected by the length of the control horizon. The latter, in turns, depends on the pointing requirements and has an impact on the control performance. For the considered sample GEO mission, it turns out that the required processing power is compatible with state-of-the-art flight qualified CPUs. A detailed investigation of the trade-off between computational burden and control performance is the subject of ongoing research.

References

- [1] Kaplan, M. H., "All-electric thruster control of a geostationary communications satellite," *Journal of Spacecraft and Rockets*, Vol. 10, No. 2, 1973, pp. 119–125. doi:10.2514/3.61856.
- [2] Zakrzwski, C., Benson, S., Sanneman, P., and Hoskins, A., "On-orbit testing of the EO-1 pulsed plasma thruster," *38th AIAA/ASME/SAE/ASEE Joint Propulsion Conference & Exhibit*, 2002. doi:10.2514/6.2002-3973.
- [3] Krøvel, T., Dörfler, F., Berger, M., and Rieber, J., "High-precision spacecraft attitude and manoeuvre control using electric propulsion," 60th International Austronautical Congress, 2009.
- [4] Nicolini, D., Robertson, D., Chesta, E., Saccoccia, G., Gibbon, D., and Baker, A. M., "Xenon resistojets as a secondary propulsion on EP spacecrafts and performance results of resistojets using Xenon," 28th International Electric Propulsion Conference, 2003.
- [5] Gessini, P., Coletti, M., Grubisic, A., Gabriel, S., Wallace, N., and Fearn, D., "Hollow cathode thruster for all-electric spacecraft," *43rd AIAA/ASME/SAE/ASEE Joint Propulsion Conference & Exhibit*, 2007. doi:10.2514/6.2007-5195.
- [6] Coletti, M., Grubisic, A., Collingwood, C., and Gabriel, S., "Electric propulsion subsystem architecture for an all-electric spacecraft," *Advances in Spacecraft Technologies*, edited by J. Hall, InTech, 2011, pp. 123–138.
- [7] Oliveira, N. and Kienitz, K., "Attitude controller design for a system using actuators with switching-time restrictions and delays," *AIAA Guidance, Navigation, and Control Conference and Exhibit*, 2000. doi:10.2514/6.2000-3967.
- [8] Dodds, S. and Williamson, S., "A signed switching time bang-bang attitude control law for fine pointing of flexible spacecraft," *International Journal of Control*, Vol. 40, No. 4, 1984, pp. 795–811. doi:10.1080/00207178408933308.
- [9] Agrawal, B., Mcclelland, R., and Song, G., "Attitude control of flexible spacecraft using pulsewidth pulse-frequency modulated thrusters," *Space Technology*, Vol. 17, No. 1, 1997, pp. 15–34. doi:10.1016/S0892-9270(97)00017-1.

- [10] Krovel, T., *Optimal tuning of PWPF modulator for attitude control*, Ph.D. thesis, Norwegian University of Science and Technology, 2009.
- [11] Doman, D., Gamble, B., and Ngo, A., "Control allocation of reaction control jets and aerodynamic surfaces for entry vehicles," *AIAA Guidance, Navigation and Control Conference and Exhibit*, 2007. doi:10.2514/6.2007-6778.
- [12] Hegrenæs, Ø., Gravdahl, J., and Tøndel, P., "Spacecraft attitude control using explicit model predictive control," *Automatica*, Vol. 41, No. 12, 2005, pp. 2107–2114. doi:10.1016/j.automatica.2005.06.015.
- [13] Vieira, M., Galvao, R., and Kienitz, K., "Attitude stabilization with actuators subject to switching-time constraints using explicit MPC," *IEEE Aerospace Conference*, 2011. doi:10.1109/aero.2011.5747482.
- [14] Sidi, M., Spacecraft dynamics and control: a practical engineering approach, Vol. 7, Cambridge university press, 2000, pp. 107–111.
- [15] Maciejowski, J., Predictive control with constraints, Pearson education, 2002, pp. 1–32.
- [16] Mayne, D., Rawlings, J., Rao, C., and Scokaert, P., "Constrained model predictive control: Stability and optimality," *Automatica*, Vol. 36, No. 6, 2000, pp. 789–814. doi:10.1016/S0005-1098(99)00214-9.
- [17] Garulli, A., Giannitrapani, A., Leomanni, M., and Scortecci, F., "Autonomous low-Earth-orbit station-keeping with electric propulsion," *Journal of Guidance Control and Dynamics*, Vol. 34, No. 6, 2011, pp. 1683–1693. doi:10.2514/1.52985.
- [18] Pittelkau, M. E., "Rotation Vector in Attitude Estimation," *Journal of Guidance, Control, and Dynamics*, Vol. 26, No. 6, 2003, pp. 855–860. doi:10.2514/2.6929.
- [19] Schneider, A., Sun, W., and Schuff, H., "The european platform LUXOR for small communications satellites," *26th International Communications Satellite Systems Conference*, 2008. doi:10.2514/6.2008-5441.
- [20] Frollani, D., Coletti, M., and Gabriel, S., "A T5 hollow cathode thruster: Experimental results and modelling," 48th AIAA/ASME/SAE/ASEE Joint Propulsion Conference & Exhibit, 2012. doi:10.2514/6.2012-4082.
- [21] Berge, S., Edfors, A., Olsson, T., Pionnier, G., Björk, M., Chasset, C., Nordebäck, T., Rieschel, M., Lübke-Ossenbeck, B., and Zentgraf, P., "Advanced AOCS design on the first Small GEO telecom satellite," 60th International Astronautical Congress, 2009.
- [22] Kim, H.-D. et al., "COMS, the new eyes in the sky for geostationary remote sensing," *Remote Sensing–Advanced Techniques and Platforms*, 2012, pp. 235–268. doi:10.5772/37926.
- [23] IBM, CPLEX, ILOG 11.0 user's manual, ILOG CPLEX Division. Incline Village, NV, 2007.